



Integrated activation strategy of mahua seed cake for efficient wastewater treatment: a sustainable approach for methylene blue removal

Himanshu Barik¹ · Md. Atif Qaiyum^{1,2} · Banashree Dey³ · Soumen Dey¹

Received: 30 March 2024 / Revised: 5 August 2024 / Accepted: 7 August 2024
© The Author(s), under exclusive licence to Springer-Verlag GmbH Germany, part of Springer Nature 2024

Abstract

The continuous search for sustainable and cost-effective water treatment solutions led to the investigation of activated mahua seed cake for wastewater treatment. The mahua seed cake was activated using hydrogen peroxide and phosphoric acid to develop an eco-friendly adsorbent. The activated material was characterized by Fourier Transform Infrared Spectroscopy (FTIR), Field Emission Scanning Electron Microscopy (FESEM), Brunauer Emmett Teller (BET) surface area analysis, and pH at zero point of charge. The results confirmed that phosphoric acid activation introduced the phosphate (PO_4^{3-}) group, as demonstrated by FTIR analysis. The FESEM micrograph revealed a very porous channel-like topology that was incredibly feasible for enhancing dye uptake. Following the adsorption of methylene blue (MB) onto phosphoric acid-modified de-oiled mahua seed (PDM), the pHzpc was found to be 7.2, confirming the material's viability in neutral pH media. The pseudo-second kinetic ($R^2=0.999$) and Langmuir isotherm models ($R^2=0.998$) were found to best describe the mechanism of interaction. The reported negative ΔG^0 value denotes the spontaneity of the scavenging process, which is endothermic and accompanied by increased randomness. Within the first 15 min, 95% of adsorption took place, and by 45 min, it reached saturation (98.25%). Inducing > 74% regeneration with dilute hydrochloric acid provided multiple-cycle reusability. Industrial wastewater was successfully treated up to 56.77%. With a neutral pH range, the material performs well with an adsorption ability of 60.15 mg/g. These findings suggest that phosphoric acid-activated mahua seed cake is a viable and sustainable option for wastewater treatment.

Keywords De-oiled mahua seed · Hydrogen peroxide · Phosphoric acid · Methylene blue · Pseudo-second-order · Langmuir isotherm

1 Introduction

The contamination of water bodies through the release of industrial wastes has led to a worldwide shortage of clean water [1, 2]. Among the best-known organic pollutants released into water bodies are dyes produced in large quantities by various industries, including textiles, dyeing,

paper, and pulp. Methylene blue (MB), a cationic dye, is used extensively for dyeing silk, leather, plastics, paper, and tanned cotton, as well as in the manufacture of paints and printing inks. In the dairy industry, it is used to determine the microbial content of milk [3]. However, acute exposure to MB can lead to shock, increased heart rate, vomiting, diarrhea, and nausea. It can lead to eye burns, which can permanently damage the eyes of humans and animals [4]. Acute exposure to MB can cause several serious health complications in both humans and animals. Clinical manifestations include cardiovascular disorders such as shock and tachycardia. Gastrointestinal symptoms include nausea, vomiting, and diarrhea, while exposure to the eyes can cause burning sensations and potentially irreversible damage. Inhalation of MB may result in tachypnea or dyspnea. Systemic effects include the development of methemoglobinemia, hemolytic anemia, and hypertensive episodes [5–9]. Various techniques

✉ Soumen Dey
soumen.dey@cuj.ac.in

¹ Environment Protection Laboratory, Department of Chemistry, Central University of Jharkhand, Cheri-Manatu, P.S. Kanke, Ranchi, India 835222

² Department of Chemistry, K. K. University, India, Nalanda

³ Department of Chemistry, The Graduate School College for Women Jamshedpur, Jamshedpur 831001, India

have been used to remove methylene blue from wastewater, including photo-electrochemical oxidation, membrane separation, advanced oxidation processes, coagulation-flocculation, and ozonation [10]. Every technology has its advantages and disadvantages. Although the advanced oxidation processes are effective, they require a high level of maintenance and incur considerable operating costs. The ion exchange method is susceptible to pH fluctuations. The electrochemical method often results in significant sludge production and carries the risk of heavy metal contamination. Although biological methods are promising, they also have their limitations, such as limited biodegradability and efficiency in certain contexts [11, 12]. Adsorption is characterized by being inexpensive, easy to implement, practical, and efficient, producing almost no toxic by-products and allowing economic recovery of the adsorbent [13, 14].

Researchers have investigated various adsorbents for MB removal in the past, emphasizing the need for new, efficient, and cost-effective materials. Goyal et al. investigated the ability of activated charcoal made from de-oiled rice bran to remove methylene blue from an aqueous solution, where the activated charcoal removed 93.7% MB in 60 min at a pH of 6 [15]. Sahu et al. investigated the potential of activated carbon prepared by carbonization of kendu fruit peels and subsequent chemical activation with ammonium carbonate to remove methylene blue, and the maximum sorption was 144.9 mg/g [16]. Belmabrouk et al. evaluated *Limoniastrum monopetalum* fruits to treat methylene blue for adsorption, and the maximum uptake was 142 mg/g [17]. Fan et al. investigated mangosteen peels. In their study, biomass-activated carbon was prepared with a dual activation method using phosphoric acid and ferric chloride. The highest biosorption capacity achieved for methylene blue was about 142 mg/g at 295 K [18]. To find a better alternative to the existing material, we aimed to explore the potential of de-oiled mahua seeds, which are extensively available in Odisha, India. The de-oiled cake, obtained after extracting the oil from the seeds, is an accessible biomass obtained from agricultural waste. In the present study, powdered de-oiled mahua seed is treated with H_2O_2 . It acts as a potent oxidant. It is also clean and reasonably priced. It is alluring to use H_2O_2 to alter the characteristics of biomaterials, since H_2O_2 may break down into clean H_2O and O_2 after use and does not produce secondary pollutants. H_2O_2 increases the cation exchange capacity of several functional groups by partially oxygenating them [19, 20]. Phosphoric acid (H_3PO_4) acts as a very effective surface-activating agent. To generate P-containing carbonaceous species (such as C–O–P), H_3PO_4 interacted with the functional groups of H_2O_2 -treated de-oiled mahua seeds, such as carbonyl groups. The accumulation of phosphate ions on the surface increases the negative charge. As a result, the total surface area of the adsorbent increases. This can also lead to the loss of vital substances such as CO and

CO_2 , creating additional holes on the surface [21–23]. Our research objective is to investigate the effectiveness of phosphoric acid-activated de-oiled mahua cake as an adsorbent for the removal of methylene blue (a cationic dye).

Thus, the primary goals of this work are (i) to elucidate the material characteristics by using FTIR, FESEM, and BET surface area; (ii) to examine the viability of PDM as a means of eliminating MB dye; (iii) to investigate the influence of various factors such as contact time, initial pH, and initial dye concentration on the adsorption capability of dyes; (iv) to carry out kinetic studies; and (v) to identify the best-suited isotherm.

2 Material and methods

2.1 Chemicals

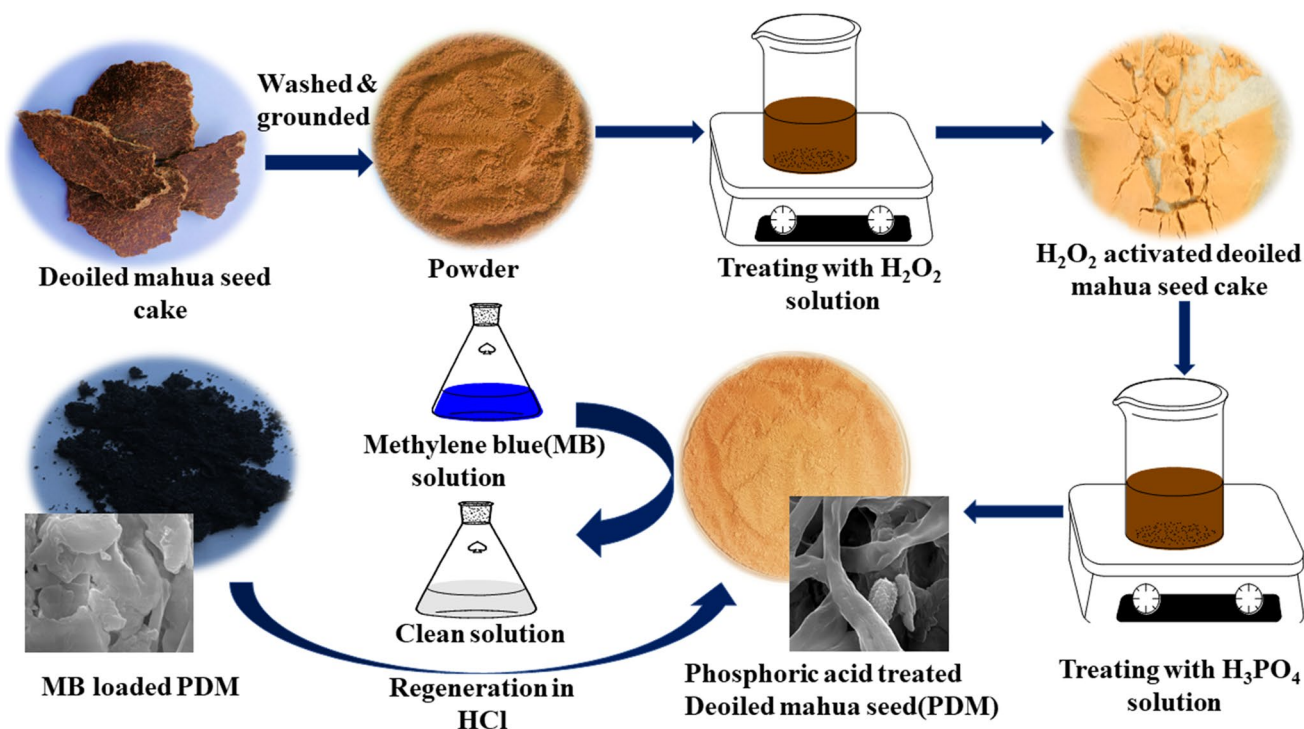
Methylene blue (98% pure) was collected from Merck Specialities Pvt. Ltd., India. Hydrochloric acid (HCl), sodium chloride (NaCl), and sodium hydroxide (NaOH) were procured from Sisco Research Laboratories Pvt. Ltd., India. Hydrogen peroxide (30%), methanol (MeOH), and phosphoric acid (84%) were purchased from Avra Synthesis Pvt. Ltd., India.

2.2 Assay and instruments

A UV–visible spectrophotometer (Hitachi, U-2900, Japan) and a pre-standardized calibration curve were employed for all colorimetric analyses. The material was ground with a Duos mixer grinder (LLMG92 500) and then dried using a Redline binder oven (RI 53). To find the pH of the solution, a pH meter (Vanira L1631) was used. The dye molecules were centrifuged using a benchtop centrifuge (Remi R-8 M). In an orbital shaking incubator (type OS 100, India), various batch experiments were carried out. The BET surface area was measured by NOVA touch 1LX. IR spectra of the PDM were obtained with FTIR (PerkinElmer, 10.4.00, USA). The surface micrographs were recorded with a FESE microscope (Zeiss electron, EVO MA 15, UK).

2.3 Preparation of phosphoric acid-modified de-oiled mahua seed (PDM)

De-oiled mahua seed cake (15 g) was put into a beaker (1 L). After adding 500 mL of distilled water to it, the mixture was agitated (Remi Electrotechnik Limited, 2MLH, India) for 6 h at 300 K. Next, the supernatant was decanted to remove all residual oil or dirt. The procedure was repeated until the supernatant was clear, and finally, the slurry was filtered. After washing the biomass with distilled water, all organic contaminants were removed with 60 mL of 30% hydrogen



Scheme 1 Preparation of phosphoric acid-modified de-oiled mahua seed (PDM) and MB adsorption

peroxide at 333 K for 12 h. The biomass was then dried at 383 K for 5 h. The treated mahua seed cake (13 g) was impregnated with phosphoric acid (84%) in a ratio of 1:2 (w/w) for 12 h at 303 K. The impregnated biomass was dried at 423 K in a muffle furnace (Thermoscientific, F48020-33–80, USA) for 5 h. It was then allowed to cool to room temperature. The biomass was purified with distilled water until the pH was neutral. It was then dried at (333 K) and named PDM (phosphoric acid-modified de-oiled mahua seed cake). This modification has been followed according to the work reported earlier [23] (Scheme 1).

2.4 Batch experiment

The optimization of various physiochemical parameters was carried out by batch studies. The adsorbent (PDM) dose (0.08 g), the volume of MB solution (30 mL), initial concentration of dye solution (10–60 mg/L), agitation period (0–60 min), and temperature variation (298–328 K) are the common conditions for the agitation experiment. The percentage of MB adsorption was 98.76% after 45 min and 99.23% after 60 min. Given the negligible increase from 45 to 60 min, the equilibration time was set at 45 min according to the energy-minimized protocol theory. 0.1 M HCl and 0.1 M NaOH solutions were used to adjust the pH. Although 98.25% adsorption was measured at pH 10, neutralization pH was maintained throughout the experiment to ensure

applicability in drinking water. Using the pH drift technique, a series of 30 mL, 0.1 M NaCl solutions were prepared; the pH of each solution was changed in the range of 4–10, and 0.08 g of PDM was added to each conical flask to determine the pH_{ZPC} of PDM. The final pH of the solutions was assessed following agitation. At a constant pH of 7.35 and a fixed contact time of 45 min, adsorption kinetics were assessed every 5 min (5, 10, 15, 20, 25, and 30 min). At four different temperatures—298 K, 308 K, 318 K, and 328 K—the adsorption isotherms were investigated using a range of dye concentrations (20, 30, 40, 50, and 60 mg/L). One hundred milliliters of MB solution ($C_0 = 100$ mg/L, pH = 7.60) and 0.08 g of PDM were combined to measure the maximum adsorption capacity. The mixture was agitated overnight. It was then centrifuged (Remi Electrotechnik Limited, R-8 M, India), and the resulting absorbance was measured to determine the ultimate concentration. The following evaluations of equilibrium adsorption uptake (q_e) and percentage of adsorption ($R\%$) were made:

$$q_e = \left(\frac{C_0 - C_e}{m} \right) v \quad (1)$$

$$R\% = \left(\frac{C_0 - C_e}{C_0} \right) \times 100 \quad (2)$$

where C_0 and C_e are initial and final concentrations (mg/L), m = amount of adsorbent (g), and v = volume of dye solution

(mL). The dye-loaded material was carefully cleaned, dried at 333 K for an overnight period, and then individually treated with a 1:1 methanol–water mixture, 0.1 M NaOH, 0.1 M HCl, and 0.1 M NaCl to assess the regeneration of MB dye-loaded spent material. The efficiency (%) was calculated using the equation:

$$\text{Efficiency (\%)} = \left(\frac{\text{Dye uptake in second run}}{\text{Dye uptake in first run}} \right) \times 100 \quad (3)$$

3 Result and discussion

3.1 Characterization

3.1.1 FTIR analysis

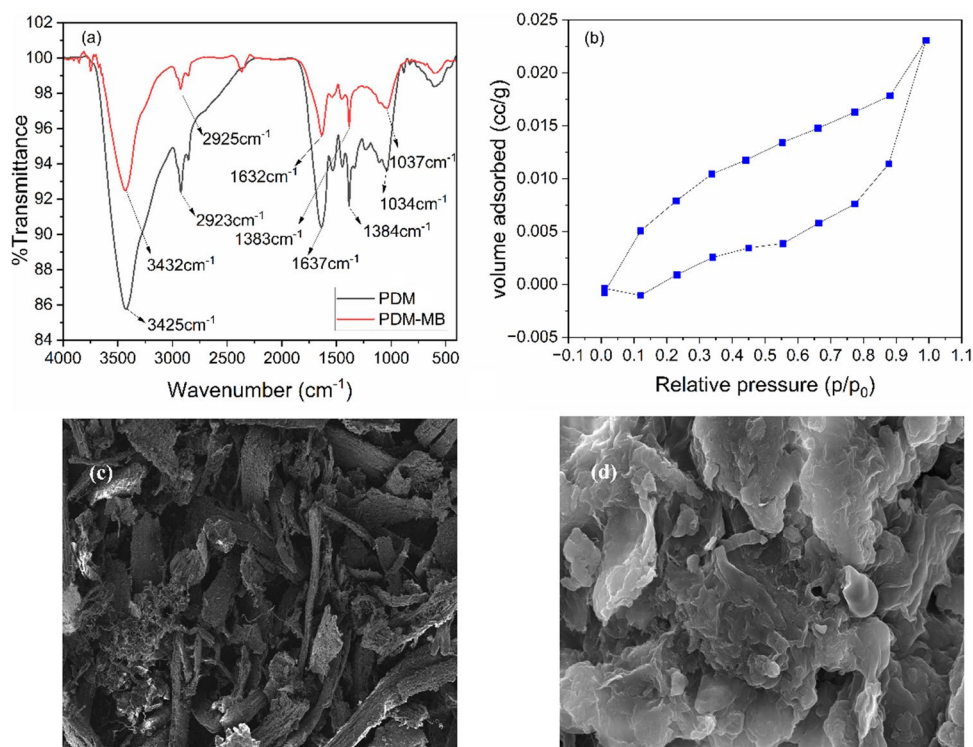
Figure 1a shows the FTIR spectra of PDM before and after MB adsorption. A sharp peak at 3425 cm^{-1} was observed, indicating the presence of N–H stretching vibrations before the adsorption of MB dye molecules. Amine groups are known to form hydrogen bonds with dye molecules, which facilitates their adsorption in PDM. After the adsorption of MB, there was a shift in the H-stretching frequency to 3432 cm^{-1} , indicating a positive interaction between PDM and the dye molecules [24]. There was evidence of vinylic and aromatic C–H stretching frequencies at 2923 cm^{-1} and 2929 cm^{-1} before and after MB adsorption on PDM,

respectively [8]. A negative shift in the carbonyl stretching of the amide group at 1632 cm^{-1} could be due to the formation of intermolecular bonds, such as hydrogen bonds. A decrease in the peak from 1384 to 1383 cm^{-1} was observed, which can be attributed to the characteristic peak of C–H bond deformation [25]. The peak at 1034 cm^{-1} was assigned to the PO_4^{3-} group [26]. FTIR analysis confirms that PDM effectively adsorbs the dye molecules. The observed changes in N–H, carbonyl, phosphate, and vinyl/aromatic C–H groups indicate significant interactions between PDM and MB. These functional groups act as active sites for adsorption and emphasize the potential of PDM as an efficient adsorbent for MB dye molecules.

3.1.2 BET surface area

Figure 1b shows the (BET isotherm) of the surface area, pore radius, and pore volume of the PDM using N_2 gas adsorption–desorption at 77.35 K. The surface area of PDM was determined to be $0.09629 \text{ m}^2/\text{g}$. The Barret-Joyner-Halenda (BJH) method is used to analyze the pore size distribution by examining the desorption isotherm of a gas. This method provides information about the pore volume and pore radius, which are crucial for understanding the porosity of the material [27]. The pore volume and pore radius were found to be $4.799 \times 10^{-3} \text{ cc/g}$ and 2.044 nm , respectively. According to the IUPAC classification, the PDM adsorption isotherm can be classified as category II [28]. There are no restrictions on monolayer-multilayer adsorption, as seen by

Fig. 1 **a** FTIR spectra of PDM before and after adsorption (black: before adsorption, red: after adsorption), **b** nitrogen adsorption–desorption curve of PDM, **c** FESEM image of PDM before adsorption of MB, **d** FESEM image of PDM after adsorption of MB



the Type II isotherm. In the initial stages of the isotherm, monolayer coverage is completely covered, and then multilayer adsorption is about to begin [29]. Considering the pore radius, PDM is assumed to have a microporous texture. The adsorption of MB molecules from the aqueous solution is facilitated by the vast number of pores [30].

3.1.3 FESEM

Figure 1c illustrates the surface morphology of PDM before adsorption of methylene blue (MB) and shows a non-uniform surface characterized by irregularities such as pits and channels. These structural features, especially the presence of pits, could enhance the adsorption efficiency by facilitating the adherence of dye molecules and providing numerous active sites for the attachment of dye molecules, potentially increasing the adsorption efficiency. After the adsorption of MB molecules, distinct changes in surface morphology were observed. As shown in Fig. 1d, the surface transforms from its initial uneven and pitted state to a more uniform, smooth, and compact structure. This change indicates that the MB molecules effectively adhere to the PDM surface and fill the existing irregularities and channels. The resulting smoother surface morphology confirms the successful adsorption of MB molecules onto PDM and emphasizes the effectiveness of the material as an adsorbent.

3.2 Adsorption studies

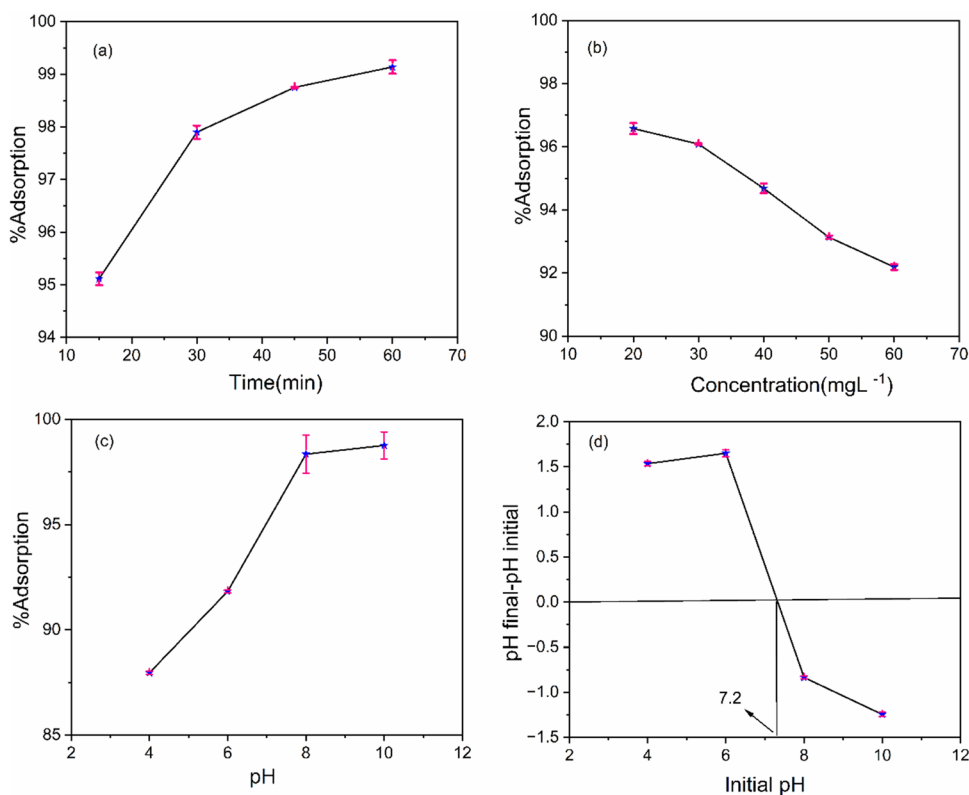
3.2.1 Effect of contact time

Figure 2a shows adsorption as a function of time. The percentage of adsorption increased initially quickly (by about 95% in the first 15 min), then steadily (98.25 to 99.23% adsorption). During the first phase of treatment, because there were many vacant sites and several functional groups on the PDM surface, they may have formed hydrogen bonds or interacted electrostatically with dye molecules, which is accounting for a high adsorption rate. With time, such sites get diminished resulting in lower uptake. So, saturation of the curve was observed [31]. All physicochemical experiments were carried out at 45 min to minimize energy consumption.

3.2.2 Effect of concentration

Figure 2b shows the effects of the initial dye concentration on the adsorption of MB on PDM. At lower concentrations, all dye molecules in the liquid phase can easily interact with the pores and channels, and they can also chemically interact with the functional groups therein. This would increase the efficiency of adsorption. Due to the saturation of the sorption sites and the prospect of slower mass transfer from the

Fig. 2 **a** Effect of time, **b** effect of concentration, **c** effect of pH, **d** effect of pH_{zpc} (initial dye concentration = 20, 30, 40, 50, and 60 mg/L; volume of dye (V) = 30 mL; contact time = 45 min; pH of the solution = 7; $T = 298$ K; agitation speed = 110 ± 5 , and adsorbent dose = 0.08 g)



aqueous phase to the solid phase, the rate of dye adsorption tends to decrease at higher concentrations [32].

3.2.3 Effect of pH and pHzpc

When the pH of the solution changes, the functional groups are protonated and deprotonated, which changes the net charge on the surface of both the adsorbent and the adsorbate [33]. This has a major influence on the adsorption of the dye. The adsorption of MB on PDM was investigated in the pH range of 4–10, as shown in Fig. 2c. The percentage of adsorption increases with the increase in pH from 4 to 10, resulting in an increase in adsorption capacity from 6.60 to 7.37 mg/g. The PDM's zero-point charge (pHzpc), which was evaluated as 7.2 in Fig. 2d, provides a clear explanation for this. The nature of the surface-active sites and the nature of the interactions between the biosorption and the MB dyes are both strongly influenced by pHzpc. A low adsorption capacity occurs at $\text{pH} < \text{pHzpc}$ because cationic dye molecules and H^+ ions are competing for the most active locations on the adsorbent's surface. The adsorbent surface becomes negatively charged when $\text{pH} > \text{pHzpc}$ facilitates the binding of cationic dyes. As a result, the adsorption percentage increases [34].

3.3 Kinetic study

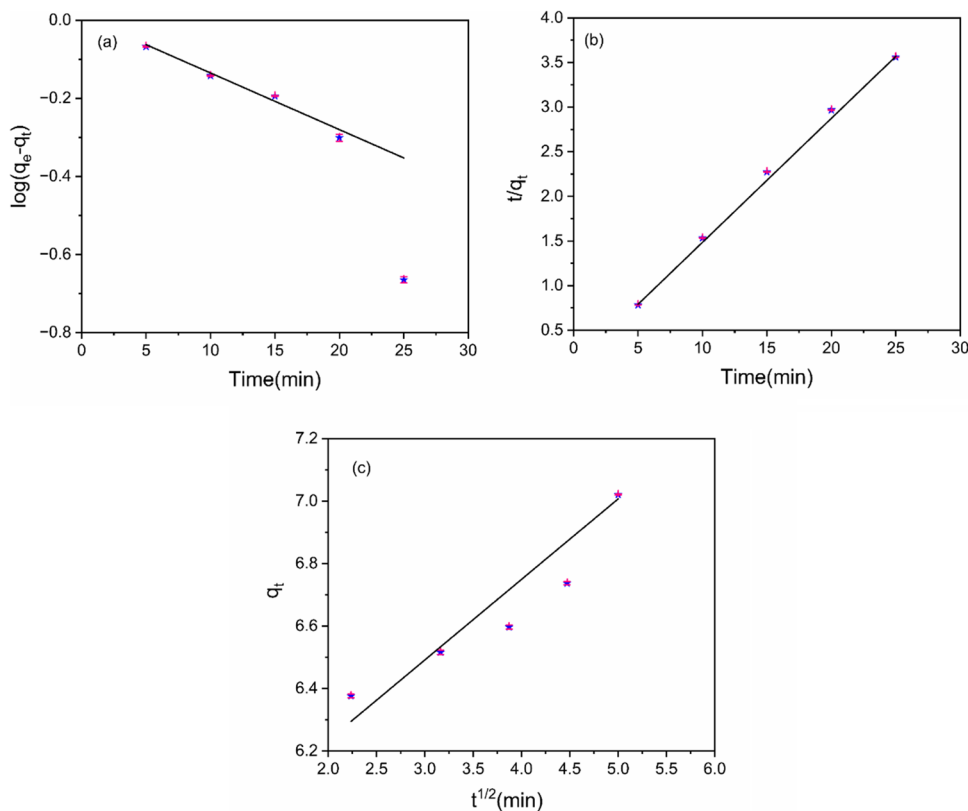
The adsorption kinetics data can predict the rate at which MB is adsorbed onto PDM and provide useful information for interpreting the adsorption mechanism [35]. Three kinetic models—pseudo-first-order, pseudo-second-order, and intraparticle diffusion—were investigated to evaluate the adsorption kinetics, as shown in Fig. 3a–c and Table 1.

In the pseudo-first-order model, the dye consumption rate is assumed to be directly proportional to the number of unoccupied sites. For adsorption in solid–liquid systems, Lagergren proposed the pseudo-first-order kinetic model [36]. Mathematically,

Table 1 Selected kinetic parameters (initial dye concentration = 20 mg/L; volume = 30 mL; contact time = (5–25) min; pH of the solution = 7.35; $T = 298$ K, agitation speed = 110 ± 5 rpm; and dose = 0.08 g)

Order	q_e (mg/g)	K	R^2
Pseudo-first-order (min^{-1})	1.023	0.033	0.722
Pseudo-second-order ($\text{mg g}^{-1} \text{min}^{-1}$)	7.211	0.199	0.999
Intraparticle diffusion ($\text{mg g}^{-1} \text{min}^{0.5}$)	7.130	0.257	0.912

Fig. 3 Kinetics of adsorption: **a** pseudo-first-order, **b** pseudo-second-order, **c** intraparticle diffusion model (initial dye concentration = 20 mg/L; volume = 30 mL; contact time = (5–25) min; pH of the solution = 7.35; $T = 298$ K, agitation speed = 110 ± 5 rpm; and dose = 0.08 g)



$$\log(q_e - q_t) = \log q_e - \left(\frac{K_1}{2.303}\right)t \tag{4}$$

The pseudo-second kinetic model predicts that the chemisorption process is the rate-limiting step, and it also implies that no mass transfer occurs in the solution [37].

Mathematically,

$$\frac{t}{q_t} = \left(\frac{1}{K_2 q_e^2}\right) + \left(\frac{t}{q_t}\right) \tag{5}$$

where the pseudo-first-order and pseudo-second-order rate constants are denoted K_1 (min^{-1}) and K_2 ($\text{mg g}^{-1} \text{min}^{-1}$) respectively.

Intraparticle diffusion affects the way that molecules from the adsorbate are transferred to the adsorbent during the diffusion process. It involves three steps. (1) Dye molecules are adsorbed externally onto the adsorbent surface; (2) progressive adsorption of dye molecules at bare spots on the adsorbent; and (3) the achievement of equilibrium [38].

Mathematically,

$$q_t = Kt^{1/2} + C \tag{6}$$

The intercept imparting boundary layer thickness is denoted by “C”, and K represents the intraparticle diffusion rate constant.

Although the findings of this investigation did not suit Lagergren’s pseudo-first-order model and intraparticle diffusion, the experimental result indicates the dynamics of the pseudo-second-order with $R^2 = 0.999$. It is clear from Table 1 that pseudo-second-order is the best option out of the three kinetic models, indicating that chemisorption is involved in the absorption of MB onto PDM.

3.4 Isotherm modeling

The adsorption isotherm depicts the equilibrium spacing of dye molecules on the adsorbent surface at a specific temperature. The calculated values and graphs are presented in Table 2 and Fig. 4 respectively. The Freundlich model, as shown in Fig. 4a, describes the multilayer adsorption on a heterogeneous surface of an adsorbent with variable binding energy and variable availability of active spots on the adsorbent’s surface [32].

The Freundlich equation is given by

$$\log q_e = \frac{1}{n} \log C_e + \log K_f \tag{7}$$

where C_e (mg/L) and q_e (mg/L) stand for equilibrium concentration and the amount of dye adsorbed per unit mass of adsorbent, respectively. K_f denotes the Freundlich constant.

The Langmuir isotherm describes the surface as homogeneous, assuming that there is no lateral interaction amongst

Table 2 Selected isotherm parameters (initial dye concentration=20, 30, 40, 50, and 60 mg/L; volume=30 mL; contact time=45 min; pH of the solution=7; $T=298$ K, 308 K, 318 K, and 328 K; agitation speed=110±5 rpm; and dose=0.08 g)

Isotherm model	Temperature (K)			
Langmuir	298	308	318	328
q_{max} (mg g ⁻¹)	28.026	31.715	41.660	50.994
b (L mg ⁻¹)	0.517	0.512	0.493	0.479
R^2	0.995	0.998	0.987	0.996
Freundlich	298	308	318	328
K_f (mg g ⁻¹)	9.564	10.770	12.153	15.288
n	2.020	2.376	2.054	1.372
R^2	0.983	0.988	0.978	0.958
Temkin	298	308	318	328
b (kJ mol ⁻¹)	0.380	0.388	0.358	0.305
K_T (L g ⁻¹)	4.463	5.175	5.573	5.983
R^2	0.991	0.998	0.993	0.911

the adsorbate’s molecules. Each site occupies only one adsorbent molecule, thus leading to monolayer formation [39]. The slope, which ranges from 0 to 1, indicates surface heterogeneity or intense adsorption. When its value approaches zero, it becomes more and more diversified.

The relevant mathematical formula is presented as

$$\frac{1}{q_e} = \frac{1}{q_m b C_o} + \frac{1}{q_m} \tag{8}$$

where q_m and b are maximum adsorption capacity and Langmuir constant, and can be determined from slope and intercept respectively from Fig. 4b.

One dimensionless constant (R_L), also referred to as the equilibrium parameter or separation factor (R_L), can be used to express the fundamental property of the Langmuir isotherm.

$$R_L = \frac{1}{1 + K_L C_o} \tag{9}$$

R_L value reveals whether adsorption is irreversible ($R_L = 0$), linear ($R_L = 1$), favorable ($0 < R_L < 1$), or unfavorable ($R_L > 1$).

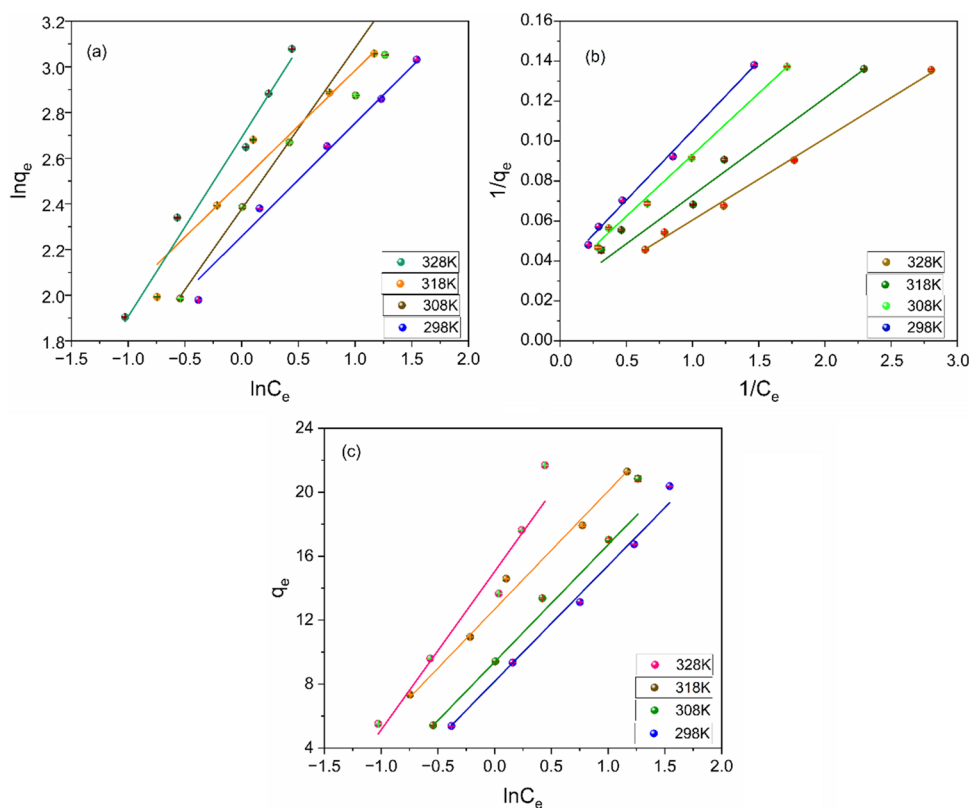
The Temkin isotherm model, as depicted in Fig. 4c, assumes indirect interaction between adsorbate–adsorbate and the heat of adsorption of all molecules decreases linearly as surface coverage progresses [40].

The Temkin equation is given by

$$q_e = B \ln K_T + B \ln C_e \tag{10}$$

$$B = \frac{RT}{b} \tag{11}$$

Fig. 4 **a** Freundlich, **b** Langmuir, **c** Temkin isotherm plots (initial dye concentration = 20, 30, 40, 50, and 60 mg/L; volume = 30 mL; contact time = 45 min; pH of the solution = 7; $T = 298$ K, 308 K, 318 K, and 328 K; agitation speed = 110 ± 5 rpm; and dose = 0.08 g)



where K_T is the equilibrium binding constant (L/g) and B (J/mol) is the Temkin constant that connects the heat of adsorption.

From Fig. 4 and Table 2, it was observed that the Langmuir model is the best fit one with the highest R^2 value, whereas the b value ranges from 0.479 to 0.517 which implies favorable adsorption. This indicates that adsorption onto the surface follows a monolayer adsorption mechanism.

3.5 Thermodynamics

Based on equilibrium data, the free energy change (ΔG^0), enthalpy change (ΔH^0), and entropy change (ΔS^0) can be calculated.

Van Hoff's equation can be used for evaluating the thermodynamic parameters.

$$\Delta G^\circ = -RT \ln(55.5 \ln K_d) \quad (12)$$

Equation 12 links further changes in Gibbs free energy to ΔH^0 and ΔS^0 .

$$\Delta G^\circ = \Delta H^\circ - T \Delta S^\circ \quad (13)$$

From Eqs. 12 and 13

$$\ln(55.5 K_d) = \frac{\Delta S^\circ}{R} - \frac{\Delta H^\circ}{RT} \quad (14)$$

where $R = 8.314 \text{ J mol}^{-1} \text{ K}^{-1}$, $K_d = \frac{q_e}{C_e}$ = distribution constant.

When $\ln(55.5) K_d$ is plotted against T^{-1} , a straight line is produced from which ΔH^0 and ΔS^0 may be calculated from the slope and intercept, in Fig. 5a, respectively and presented in Table 3 [41].

From Table 3 the negative value of ΔG^0 indicates that the adsorption process is spontaneous and thermodynamically advantageous. The increase in the negative value of ΔG^0 with temperature suggests that elevated temperatures are advantageous for the adsorption process. A positive ΔH^0 value confirmed that the adsorption of MB is endothermic. An increase in randomness at the dye adsorption site is affirmed by a positive ΔS^0 value.

3.6 Activation energy

According to the Arrhenius equation, the activation energy (E_a) connected to the adsorption of MB onto PDM as shown in Fig. 5b was calculated and presented in Table 4 as follows:

$$\ln K_a = \ln A - \frac{E_a}{RT} \quad (15)$$

Modified Arrhenius equation related to surface coverage (θ) is represented by

Fig. 5 a Van't Hoff plot, **b** Arrhenius plot (initial dye concentration = 20, 30, 40, 50, and 60 mg/L; volume = 30 mL; contact time = 45 min; pH of the solution = 7; $T = 298$ K, 308 K, 318 K, and 328 K; agitation speed = 110 ± 5 rpm; and dose = 0.08 g)

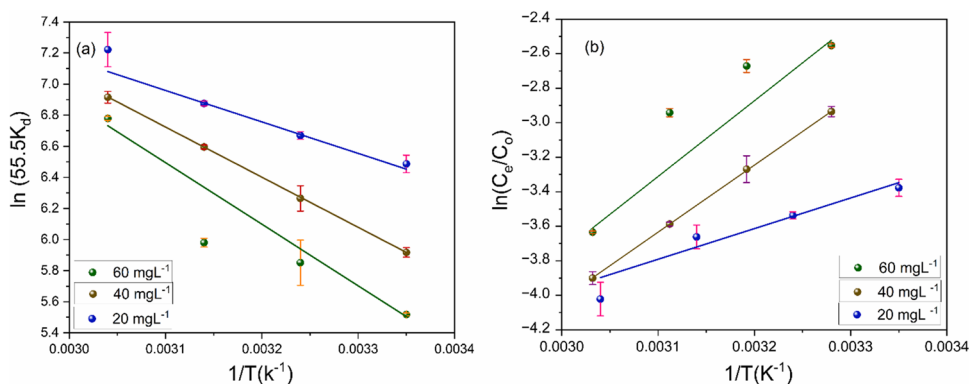


Table 3 Selected thermodynamic parameters (initial dye concentration = 20, 30, 40, 50, and 60 mg/L; volume = 30 mL; contact time = 45 min; pH of the solution = 7; $T = 298$ K, 308 K, 318 K, and 328 K; agitation speed = 110 ± 5 rpm; and dose = 0.08 g)

Concentration (mg/L)	Temperature (K)	ΔG (kJ/mol)	ΔH (kJ/mol)	ΔS (kJ/mol/K)
20	298	-15.685	15.157	0.103
	308	-16.720		
	318	-17.755		
	328	-18.790		
40	298	-14.603	26.819	0.139
	308	-15.993		
	318	-17.383		
	328	-18.773		
60	298	-13.285	29.627	0.144
	308	-14.725		
	318	-16.165		
	328	-17.605		

Table 4 Activation energy at various concentrations (initial dye concentration = 20, 30, 40, 50, and 60 mg/L; volume = 30 mL; contact time = 45 min; pH of the solution = 7; $T = 298$ K, 308 K, 318 K, and 328 K; agitation speed = 110 ± 5 rpm; and dose = 0.08 g)

Concentration (mg/L)	Temperature (K)	Activation energy (E_a) (kJ/mol)	θ
20	298	14.758	0.965
	308		0.970
	318		0.975
	328		0.982
40	298	25.853	0.946
	308		0.961
	318		0.972
	328		0.979
60	298	29.139	0.922
	308		0.931
	318		0.947
	328		0.973

$$S^* = (1 - \theta)e^{-\frac{E_a}{RT}} \tag{16}$$

$$\theta = \left(1 - \frac{C_e}{C_0}\right) \tag{17}$$

where A denotes the preexponential factor, E_a (kJ/mol) is the activation energy, T refers to the operation temperature (K), R represents the universal gas constant (8.314 J/molK), S^* is the adsorbate/adsorbent function, and θ represents the surface area coverage. S^* should lie between $0 < S^* < 1$. The value of E_a indicates whether an adsorption phenomenon is physical or chemical [42].

From Table 4, the value of activation energy varies from 14.758 to 29.139 kJ/mol, which signifies physisorption. At concentrations of 20 mg/L, 40 mg/L, and 60 mg/L, the highest θ value (surface coverage) are found to be 0.982, 0.979, and 0.973, respectively at 328 K, suggesting favorable adsorption at a higher temperature.

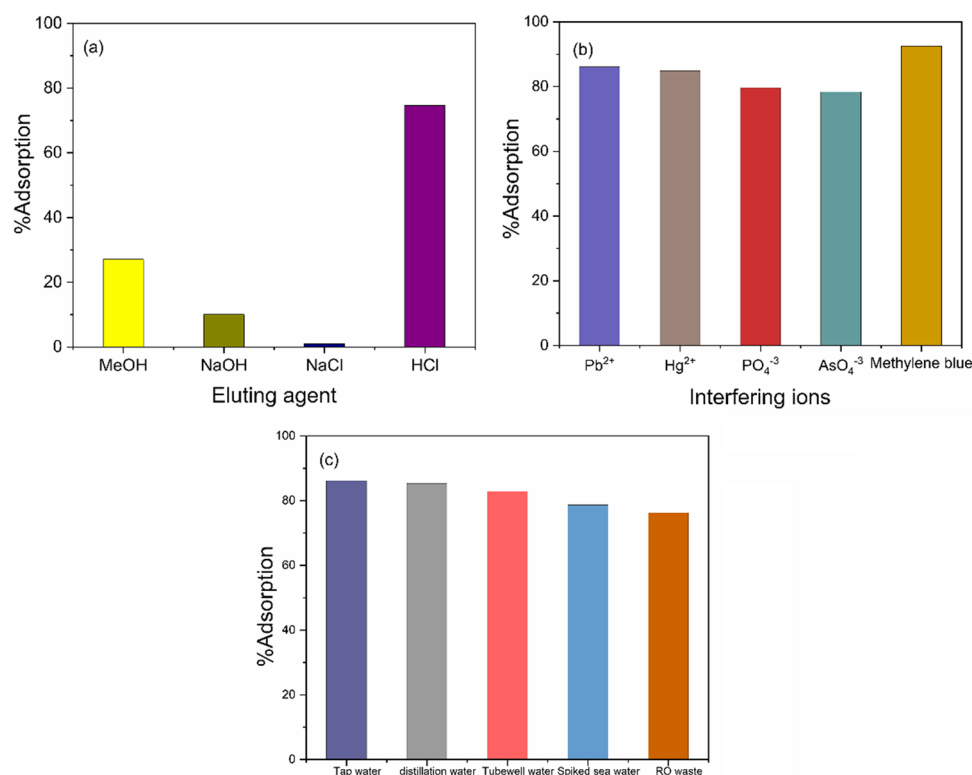
3.7 Regeneration and reuse

To improve sustainability, an adsorbent must maintain its effectiveness over several cycles. Various media were tested to regenerate the exhausted PDM: hydrochloric acid (0.1 M), sodium hydroxide (0.1 M), sodium chloride (0.1 M), and a 1:1 methanol–water mixture. Figure 6a shows that the highest regeneration (74.65%) was achieved in an acidic solution, consistent with H^+ exchange occurring with the dye binding sites. The substance was carefully cleaned before being tested for additional efficacy. The material can be recycled up to four times without significant loss of activity.

3.8 Influence of coexisting ions

To evaluate the PDM's real-time dye elimination efficacy, a tiny quantity of heavy metals and ions (Hg^{2+} , Pb^{2+} , PO_4^{3-} , AsO_4^{3-}) were introduced, as the wastewater itself has different levels of dissolved salt and heavy metals in it. The MB adsorption was examined in the presence of four ions,

Fig. 6 **a** Regeneration of PDM, **b** adsorption capacity in the presence of interfering ions, **c** effect of different spiked effluents (initial dye concentration = 20 mg/L; volume = 30 mL; contact time = 45 min; pH of the solution = 7; $T = 298$ K; agitation speed = 110 ± 5 rpm; and dose = 0.08 g)



such as Hg^{2+} (1 mg/L), Pb^{2+} (1 mg/L), PO_4^{3-} (1 mg/L), and AsO_4^{3-} (0.5 mg/L), to evaluate any effects of this nature. Individual ion concentrations were selected by WHO/EPA [43, 44]. In Fig. 6b, PDM exhibits 92.5% MB adsorption in the absence of any ions, and this is slightly decreased to 86.1% and 84.9% in the presence of cations. This decline can be attributed to the fact that MB itself is a cationic dye and in the presence of cationic ions (Hg^{2+} and Pb^{2+}) there may be competitive inhibition, preventing the adsorption of dye molecules by the material. However, 79.6% and 78.35% of adsorption were observed in the presence of PO_4^{3-} and AsO_4^{3-} respectively. It can be concluded that phosphate and arsenate ions have higher competitive properties than cations. On the contrary, cations like lead (Pb^{2+}) and mercury (Hg^{2+}) have an insignificant effect.

3.9 Influence of spiked effluents

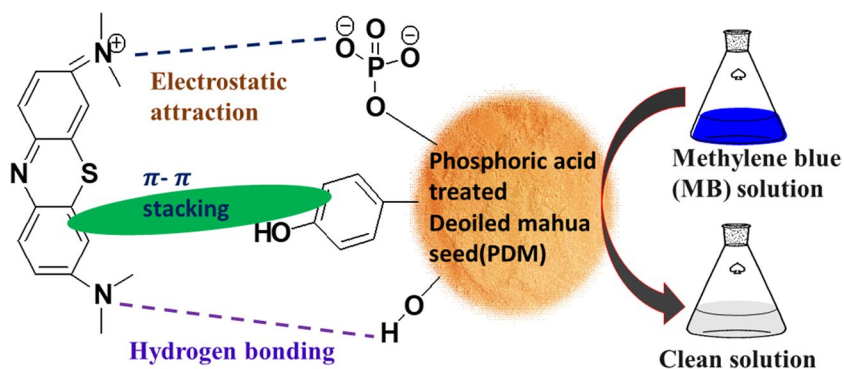
To better understand the practical applicability, four different sources of spiked wastewater—RO wastewater, distillation plant wastewater, tube well water, spiked seawater, and tap water—were selected and shown in Fig. 6c. Their pH values were 6.72, 7.78, 7.18, 6.90, and 8.19. The mixture was then treated with 20 mg/L dye, and the percentage of adsorption was calculated. The presence of various ions and impurities only slightly affected the adsorption rate in these spiked wastewaters. In contrast to RO wastewater, which had the

lowest percentage of adsorption (76.18%), tap water had the highest percentage of adsorption (86.07%). This experiment is also confirmed by our previously discussed pH experiments, which show that as the pH increases, the percentage of adsorption also increases.

3.9.1 Industrial effluent

To figure out how effectively PDM works in treating wastewater in real-life situations, a batch experiment was carried out. This helps in understanding how PDM would perform in actual wastewater treatment plants, where the composition of wastewater can vary widely. From local Arvind textile industries, wastewater that was discharged after the dyeing of cloths was gathered. It was centrifuged and filtered. The fluid was diluted 60 times to reduce its concentration. After 45 min of stirring, 0.08 g of PDM was combined with 30 mL of effluent solution, and the final concentration was determined; 56.77% removal indicates that the adsorption characteristics were significantly diminished in the presence of additional ions and dyes, which can also be used for practical purposes [45]. The experiment opens up avenues for further research into improving the effectiveness of PDM or exploring alternative treatment methods that can address the challenges posed by complex wastewater compositions.

Fig. 7 Mechanism of adsorption



3.10 Mechanism of adsorption

According to the FTIR study, the surface of PDM has functional groups such as carbonyl ($-C=O$) and amine ($-NH$). The mechanism of the adsorption process is supported by these functional groups. Through the process of phosphorylation, the acidic PO_4^{3-} group was formed on the surface of PDM by electrostatic interaction, which facilitates the adsorption process of the cationic MB dye. The electrostatic attraction causes the cationic dye to cling to the surface of the adsorbent above pH_{ZPC} [46]. The $-OH$ and $-COOH$ on the surface and the N-atom of the cationic MB create hydrogen bonds as additional interactions on the surface of PDM. Additionally, the contact between the aromatic rings of PDM surfaces and the phenyl rings of MB can be enabled by π - π stacking, as shown in Fig. 7, and the lower removal is facilitated by the coulombic resistance between PDM and dyes below pH_{ZPC} [47, 48].

3.11 Comparison of PDM with another adsorbent

If a new material outperforms the materials currently in use, it can be considered promising. The surface area, the incorporation of active sites, and the water stability of natural components are usually increased by chemical treatment.

These improvements increase the ability of an adsorbent to bind dyes. Table 5 summarizes the comparative study of the maximum uptake of several sorbents, including PDM. Wang et al. examined the potential of peanut shells, treated with citric acid and used as an adsorbent for the removal of MB from aqueous solutions; 64.5% removal rate of MB was achieved at pH 4, adsorbent dosage (0.1 g), and initial dye concentration (100 mg/L), and biosorption isotherms revealed that the citric acid-activated peanut shell exhibited MB uptake of 120.8 mg/g, as per the Langmuir model [49]. Hevira et al. examined the performance of the biosorbent from *Terminalia catappa* (TC) shells for the removal of MB from aqueous solutions. The optimal conditions for the uptake of MB from *Terminalia catappa* shells were observed at a pH of 5, a contact time of 45 min, and an initial dye concentration of 800 mg/L, resulting in a maximum adsorption capacity of 88.62 mg/g. The examination of adsorption isotherm and kinetics study demonstrated that the MB uptake was best to the Freundlich and pseudo-second-order models respectively [50]. Holliday et al. observed that pea waste had a maximum potential adsorption capacity of 167 mg/g, demonstrating a notable superiority over similar bio-adsorbent investigations in recent times; 89% MB was successfully removed using 0.1 g of biosorbent. The most suitable model for describing the

Table 5 Comparative adsorption efficiency of various agricultural wastes for MB adsorption from water

Adsorbent	Contact time (min)	Dose (g)	Dye concentration (mg/L)	pH	Adsorption capacity (mg/g)	Reference
Citric acid-activated peanut shell	120	0.1	100	4	120.4	[49]
<i>Terminalia catappa</i> shell	45	0.1	800	5	88.62	[50]
Pea waste	240	0.5	50	10	167.0	[51]
Sugarcane bagasse	1440	2	5	-	9.410	[52]
<i>Ficus palmata</i> leaves	80	0.15	15	7	6.900	[53]
Treated peanut hull	6	1	100	6	132.0	[54]
<i>Agrobacterium fabrum</i> biomass	60	1	200	11	91.00	[55]
PDM	45	0.08	20	7	60.15	This study

adsorption process was found to be pseudo-second-order adsorption kinetic and Freundlich adsorption isotherm model [51]. Andrade Siqueira et al. found that *Sugarcane bagasse* exhibited a maximum MB adsorption capacity of 9.41 mg/g at 318 K after 24 h of contact period. Analysis of adsorption kinetics favored the pseudo-second-order model, suggesting a chemical process was involved [52]. Fiaz et al. observed that *Ficus palmata* leaves achieved maximum MB removal efficiency of 98%. This was accomplished by agitating 0.45 g of adsorbent with an initial dye concentration of 15 mg/L for 80 min at 318 K and pH = 7 [53]. Lv et al. evaluated the Fenton-like treated peanut hull for the removal of MB. Fenton-like treated peanut hull was found to have an 85.1% MB removal rate under optimal conditions of pH 6.0, an initial dye concentration of 100 mg/L, and an adsorbent dosage of 1.0 g/L. The adsorption mechanism followed pseudo-second-order models, Redlich-Peterson and Langmuir models [54]. Sharma et al. examined the sorption capacity of MB using *Agrobacterium fabrum* biomass, and the observed maximum adsorption capacity for MB was 91 mg/g at pH = 11 and 200 mg/L dye concentration [55]. 98.25% MB uptake within 45 min (adsorbent dose = 0.08 g and $C_0 = 20$ mg/L) supported with an adsorption capacity of 60.15 mg/g demonstrates the brilliance of the PDM at a neutral pH range.

4 Conclusion

Methylene blue (MB) can be effectively removed from wastewater using phosphoric acid-modified de-oiled mahua seed cake (PDM). FTIR analysis shows the presence of active $-NH$ groups. The surface area of PDM was determined to be 0.09629 m^2/g . FESEM shows a non-uniform surface with irregularities such as pits and grooves. The zero-point charge (pH_{zpc}) of PDM was determined to be 7.2. The adsorption kinetics follows a pseudo-second-order model, indicating a chemisorptions process. The Langmuir isotherm model fits best and confirms monolayer and homogeneous adsorption. The maximum adsorption capacity was determined to be 60.15 mg/g at neutral pH. The overall interaction proved to be feasible, endothermic, and spontaneous. The spent material can be regenerated with a diluted HCl solution up to 74.65% and reused for up to four cycles. Compared to other adsorbents, PDM shows significant potential for dye removal. Industrial wastewater trials have demonstrated its superior applicability and usage. However, this study is limited to MB removal, and future research should investigate the removal of other dyes. For comprehensive field implementation, column experiments should be conducted to examine the effects of various parameters such as bed height, flow rate, and contact time. Additionally, future

studies could explore heavy metal removal and the magnetization of PDM. From the above results discussed, it can be said that PDM could be an economically feasible and cost-effective adsorbent for the removal of dyes from wastewater albeit not general. Although a lot has been done in this area, the disposal issue remained a challenge and untouched one. It should be taken up as priority areas.

In a nutshell, the present work highlights the efficacy of a highly abundant biomass for an economic water treatment without harming the environment. Mild chemical activation of a potential phytomass namely *Nelumbo nucifera* has been highlighted to act as a scavenger for toxic dyes from aqueous body.

Supplementary Information The online version contains supplementary material available at <https://doi.org/10.1007/s13399-024-06040-z>.

Acknowledgements M.A.Q. thanks the Central University of Jharkhand for the fellowship.

Author contribution Himanshu Barik: wrote the original manuscript, methodology, and artwork; Md. Atif Qaiyum: data curation and validation; Banashree Dey: formal analysis and review; Soumen Dey: conceptualization, review, editing, and overall supervision.

Data availability Data will be made available upon reasonable request.

Declarations

Conflict of interest The authors declare no competing interests.

References

1. Singh AK, Mishra S, Singh JK (2019) Underwater superoleophobic biomaterial based on waste potato peels for simultaneous separation of oil/water mixtures and dye adsorption. *Cellulose* 26(9):5497–5511. <https://doi.org/10.1007/s10570-019-02458-1>
2. Saravanan A, Kumar PS, Jeevanantham S, Karishma S, Tajsabreen B, Yaashikaa PR, Reshma B (2021) Effective water/wastewater treatment methodologies for toxic pollutants removal: processes and applications towards sustainable development. *Chemosphere* 280:130595. <https://doi.org/10.1016/j.chemosphere.2021.130595>
3. Chowdhury S, Saha PD (2012) Biosorption of methylene blue from aqueous solutions by a waste biomaterial: hen feathers. *Appl Water Sci* 2:209–219. <https://doi.org/10.1007/s13201-012-0039-0>
4. Vutskits L, Briner A, Klauser P, Gascon E, Dayer A, Kiss J, Muller D, Licker M, Morel D (2008) Adverse effects of methylene blue on the central nervous system. *Anesthesiology* 108:684–692. <https://doi.org/10.1097/ALN.0b013e3181684be4>
5. Dbik A, Bentahar S, El Messaoudi N, El Khomri M, Lacherai A (2020) Removal of methylene blue from aqueous solution by tunics of the corm of the saffron. *Iran J Chem Chem Eng* 39(6):95–104
6. Mabungela N, Shooto ND, Mtunzi F, Naidoo EB, Kyzas G (2022) The adsorption of copper, lead metal ions, and methylene blue dye from aqueous solution by pure and treated fennel. *Adsorp sci technol*. <https://doi.org/10.1155/2022/5787690>
7. Shi C, Tao F, Cui Y (2018) Evaluation of nitriloacetic acid modified cellulose film on adsorption of methylene blue. *Int J Biol*

- Macromol 114:400–407. <https://doi.org/10.1016/j.ijbiomac.2018.03.146>
8. Sakr F, Alahiane S, Sennaoui A, Dinne M, Bakas I, Assabbane A (2020) Removal of cationic dye (Methylene Blue) from aqueous solution by adsorption on two types of biomaterials of South Morocco. *Mater Today Proc* 22:93–96. <https://doi.org/10.1016/j.matpr.2019.08.101>
 9. Holliday MC, Parsons DR, Zein SH (2024) Agricultural pea waste as a low-cost pollutant biosorbent for methylene blue removal: adsorption kinetics, isotherm and thermodynamic studies. *Biomass Convers Biorefin* 14:6671–6685. <https://doi.org/10.1007/s13399-022-02865-8>
 10. Dehghani MH, Karimi B, Rajaei MS (2016) The effect of aeration on advanced coagulation, flotation, and advanced oxidation processes for color removal from wastewater. *J Mol Liq* 223:75–80. <https://doi.org/10.1016/j.molliq.2016.08.019>
 11. Grabi H, Lemlikchi W, Derridj F, Lemlikchi S, Trari M (2021) Efficient native biosorbent derived from agricultural waste precursor for anionic dye adsorption in synthetic wastewater. *Biomass Convers Biorefin* 13:1–18. <https://doi.org/10.1007/s13399-021-01280-9>
 12. Nayak SS, Mirgane NA, Shivankar VS, Pathade KB, Wadhawa GC (2021) Adsorption of methylene blue dye over activated charcoal from the fruit peel of plant *Hydnocarpus pentandra*. *Mater Today Proc* 37:2302–2305. <https://doi.org/10.1016/j.matpr.2020.07.728>
 13. Wekoye JN, Wanyonyi WC, Wangila PT, Tonui MK (2020) Kinetic and equilibrium studies of Congo red dye adsorption on cabbage waste powder. *J Environ Chem Ecotoxicol* 2:24–31. <https://doi.org/10.1016/j.enceco.2020.01.004>
 14. Ajani AO, Dada EO, Olu-arotowa OA, Okeowo I (2019) Adsorption of methylene blue from aqueous solution using microwave-assisted BaCl₂ modified activated carbon produced from mango seed shell. *Adsorption* 3(1). [https://doi.org/10.36108/laujoces/9102/20\(0270\)](https://doi.org/10.36108/laujoces/9102/20(0270))
 15. Goyal C, Kaushik D, Arora R, Goyal SB (2020) Removal of methylene blue dye from aqueous solution using de-oiled rice bran as adsorbent. *Int J Adv Sci Technol* 29:723–730
 16. Sahu S, Pahi S, Sahu JK, Sahu UK, Patel RK (2020) Kendu (*Diospyros melanoxylon Roxb*) fruit peel activated carbon—an efficient bioadsorbent for methylene blue dye: equilibrium, kinetic, and thermodynamic study. *Environ Sci Pollut* 27:22579–22592. <https://doi.org/10.1007/s11356-020-08561-2>
 17. Belmabrouk H, Brahem RA, Bajahzar A et al (2022) Low-cost *Limoniastrum monopetalum* fruits as efficient biosorbent of methylene blue from aqueous suspension. *Biomass Convers Biorefin* 14(8):9151–9162. <https://doi.org/10.1007/s13399-022-02968-2>
 18. Fan Z, Zhang Z, Zhang G et al (2022) Phosphoric acid/FeCl₃ converting waste mangosteen peels into bio-carbon adsorbents for methylene blue removal. *Int J Environ Sci Technol* 19:12315–12328. <https://doi.org/10.1007/s13762-022-03952-z>
 19. Zhang Y, Zheng Y, Yang Y, Huang J, Zimmerman AR, Chen H, Gao B (2021) Mechanisms and adsorption capacities of hydrogen peroxide modified ball milled biochar for the removal of methylene blue from aqueous solutions. *Bioresour Technol* 337:125432. <https://doi.org/10.1016/j.biortech.2021.125432>
 20. Huff MD, Lee JW (2016) Biochar-surface oxygenation with hydrogen peroxide. *J Environ Manage* 165:17–21. <https://doi.org/10.1016/j.jenvman.2015.08.046>
 21. Ajaelu CJ, Adetoye OA (2023) Liquid-phase adsorption of methylene blue on functionalized *Solanum macrocarpon* calyx activated carbon: kinetics, equilibrium, and thermodynamic studies. *Int J Environ Sci Technol* 20(4):3953–3964. <https://doi.org/10.1007/s13762-023-04829-5>
 22. Neme I, Gonfa G, Masi C (2022) Preparation and characterization of activated carbon from castor seed hull by chemical activation with H₃PO₄. *Materials* 15:100304. <https://doi.org/10.1016/j.rinma.2022.100304>
 23. Khan TA, Khan EA (2016) Adsorptive uptake of basic dyes from aqueous solution by novel brown linseed deoiled cake activated carbon: equilibrium isotherms and dynamics. *J Environ Chem Eng* 4(3):3084–3095. <https://doi.org/10.1016/j.jece.2016.06.009>
 24. Choudhury S, Ray SK (2018) Efficient removal of cationic dye mixtures from water using a bio-composite adsorbent optimized with response surface methodology. *Carbohydr Polym* 200:305–320. <https://doi.org/10.1016/j.carbpol.2018.07.080>
 25. Tsai WC, de Luna, MDG, Bermillo-Arriegasdo HLP, Futralan CM, Colades JL, Wan MW (2016) Competitive fixed-bed adsorption of Pb (II), Cu (II), and Ni (II) from aqueous solution using chitosan-coated bentonite. *Int J Polym Sci* 2016:1–11. <https://doi.org/10.1155/2016/1608939>
 26. Sahibed-dine A, Bentiss F, Bensitel M (2017) The photocatalytic degradation of methylene blue over TiO₂ catalysts supported on hydroxyapatite. *J Mater* 8(4):1301–1311
 27. Sonwane CG, Bhatia SK (2000) Characterization of pore size distributions of mesoporous materials from adsorption isotherms. *J Phys Chem B* 104(39):9099–9110. <https://doi.org/10.1021/jp000907j>
 28. Leão TP, Tuller M (2014) Relating soil specific surface area, water film thickness, and water vapor adsorption. *Water Resour Res* 50(10):7873–7885. <https://doi.org/10.1002/2013WR014941>
 29. Muttakin M, Mitra S, Thu K, Ito K, Saha BB (2018) Theoretical framework to evaluate minimum desorption temperature for IUPAC classified adsorption isotherms. *Int J Heat Mass Transf* 122:795–805. <https://doi.org/10.1016/j.ijheatmasstransfer.2018.01.107>
 30. Nasrullah A, Saad B, Bhat AH, Khan AS, Danish M, Isa MH, Naeem A (2018) Mangosteen peel waste as a sustainable precursor for high surface area mesoporous activated carbon: characterization and application for methylene blue removal. *J Clean Prod* 211:1190–1200. <https://doi.org/10.1016/j.jclepro.2018.11.094>
 31. Qaiyum MA, Priyadarsini Samal P, Dey B, Dey S (2023) Elegant synthesis of phyto-magnetic Fe₃O₄@ *Syzygium cumini* and its application for decontamination of Eriochrome Black T dye from aqueous solution and wastewater. *Biomass Conv Bioref* 1–20. <https://doi.org/10.1007/s13399-023-04372-w>
 32. Jain R, Sikarwar S (2014) Adsorption and desorption studies of Congo red using low-cost adsorbent: activated de-oiled mustard. *Desalination Water Treat* 52(37–39):7400–7411. <https://doi.org/10.1080/19443994.2013.837004>
 33. Hermann DT, Tome S, Shikuku VO, Tchuigwa JB, Spieß A, Janiak C, Joh Dina DD (2022) Enhanced performance of hydrogen peroxide modified pozzolan-based geopolymer for abatement of methylene blue from aqueous medium. *Silicon* 14(10):5191–5206. <https://doi.org/10.1007/s12633-021-01264-4>
 34. Sethi GK, Qaiyum MA, Samal PP, Dutta S, Dey B, Dey S (2023) Designed synthesis of phyto-magnetic and techno-economic peanut-shell embedded ferrite as a classic scavenger for recalcitrant crystal violet from wastewater. *Biomass Conv Bioref* 1–12. <https://doi.org/10.1007/s13399-023-04461-w>
 35. Abd El-Latif M, El L, Ibrahim EM (2009) Adsorption equilibrium, kinetics and thermodynamics of methylene blue from aqueous solutions using biopolymer oak sawdust composite. *J Am Chem Soc* 6(6):267–283
 36. Salahudeen N, Alhassan A (2022) Adsorption of crystal violet on rice husk activated carbon. *J Eng Sci* 9(1):F11–F15. [https://doi.org/10.21272/jes.2022.9\(1\).f2](https://doi.org/10.21272/jes.2022.9(1).f2)
 37. Arici TA (2021) CTAB/H₂O₂ modified biosorbent for anionic dye from aqueous solutions: biosorption parameters and mechanism. *Biomass Conv Bioref* 13:10689–10699. <https://doi.org/10.1007/s13399-021-01920-0>

38. Kumari R, Khan MA, Mahto M, Qaiyum MA, Mohanta J, Dey B, Dey S (2020) Dewaxed honeycomb as an economic and sustainable scavenger for malachite green from water. *ACS Omega* 5(31):19548–19556. <https://doi.org/10.1021/acsomega.0c02011>
39. Farnane M, Machrouhi AICHA, Elhalil ALAÂEDDINE, Abden-nouri M, Qourzal S, Tounsadi HANANE, Barka NOUREDDINE (2018) New sustainable biosorbent based on recycled deoiled carob seeds: optimization of heavy metals remediation. *J Chem.* <https://doi.org/10.1155/2018/5748493>
40. Renita AA, Kumar PS, Jabasingh SA (2019) Redemption of acid fuchsin dye from wastewater using de-oiled biomass: kinetics and isotherm analysis. *Bioresour Technol Rep* 7:100300. <https://doi.org/10.1016/j.biteb.2019.100300>
41. Lima EC, Gomes AA, Tran HN (2020) Comparison of the non-linear and linear forms of the Van't Hoff equation for calculation of adsorption thermodynamic parameters (ΔS° and ΔH°). *J Mol Liq* 311:113315. <https://doi.org/10.1016/j.molliq.2018.10.048>
42. Jain SN, Garud VB, Dawange SD, Sonawane DD, Shaikh ER (2022) Sesame (*Sesamum indicum*) oil cake—industrial waste biomass for sequestration of Basic Blue 26 from aqueous media. *Biomass Convers Biorefin* 12(9):3783–3793
43. Bendicho C, Lavilla I, Pena-Pereira F, De La Calle I, Romero V (2021) Nanomaterial-integrated cellulose platforms for optical sensing of trace metals and anionic species in the environment. *Sensors* 21(2):604. <https://doi.org/10.3390/s21020604>
44. Bhat A, Hara TO, Tian F, Singh B (2023) Review of analytical techniques for arsenic detection and determination in drinking water. *Env Sci Adv* 2(2):171–195. <https://doi.org/10.1039/D2VA00218c>
45. Rout A, Qaiyum MA, Samal PP, Dutta S, Dey B, Dey S (2023) Brinjal (*Solanum melongena*) stalk waste as an effective scavenger for Eriochrome Black-T from water and wastewater: an approach towards waste to best. *Int J Phytoremediation* 25(8):956–964. <https://doi.org/10.1080/15226514.2022.2123445>
46. Ngulube T, Gumbo JR, Masindi V, Maity A (2017) An update on synthetic dye adsorption onto clay-based minerals: a state-of-art review. *J Environ Manage* 191:35–57. <https://doi.org/10.1016/j.jenvman.2016.12.031>
47. Li Y, Yang CX, Qian HL, Zhao X, Yan XP (2019) Carboxyl-functionalized covalent organic frameworks for adsorption and removal of triphenylmethane dyes. *ACS Appl Nano Mater* 2(11):7290–7298. <https://doi.org/10.1021/acsnm.9b01781>
48. Deokar SK, Mandavgane SA, Kulkarni BD (2016) Adsorptive removal of 2,4-dichlorophenoxyacetic acid from aqueous solution using bagasse fly ash as adsorbent in batch and packed-bed techniques. *Clean Techn Environ Policy* 18:1971–1983. <https://doi.org/10.1007/s10098-016-1124-0>
49. Wang P, Ma Q, Hu D, Wang L (2016) Adsorption of methylene blue by a low-cost biosorbent: citric acid modified peanut shell. *Desalination Water Treat* 57(22):10261–10269. <https://doi.org/10.1080/19443994.2015.1033651>
50. Hevira L, Ighalo JO, Aziz H, Zein R (2021) Terminalia catappa shell as low-cost biosorbent for the removal of methylene blue from aqueous solutions. *J Ind Eng Chem* 97:188–199. <https://doi.org/10.1016/j.jiec.2021.01.028>
51. Holliday MC, Parsons DR, Zein SH (2024) Agricultural pea waste as a low-cost pollutant biosorbent for methylene blue removal: adsorption kinetics, isotherm, and thermodynamic studies. *Biomass Convers Biorefin* 14(5):6671–6685. <https://doi.org/10.1007/s13399-022-02865-8>
52. Andrade Siqueira TC, Zanette da Silva I, Rubio AJ, Bergamasco R, Gasparotto F, de Souza A, Paccola E, Ueda Yamaguchi N (2020) Sugarcane bagasse as an efficient biosorbent for methylene blue removal: kinetics, isotherms and thermodynamics. *Int J Environ Res Public Health* 17(2):526. <https://doi.org/10.3390/ijerph17020526>
53. Fiaz R, Hafeez M, Mahmood R (2019) Ficus palmata leaves as a low-cost biosorbent for methylene blue: thermodynamic and kinetic studies. *Water Environ Res* 91(8):689–699. <https://doi.org/10.1002/wer.1093>
54. Lv D, Jiang G, Li C, Zhu Q, Wang Z (2022) Ultrafast removal of methylene blue from water by Fenton-like pretreated peanut hull as biosorbent. *Green Chem Lett Rev* 15(1):93–107. <https://doi.org/10.1080/17518253.2021.2024277>
55. Sharma S, Hasan A, Kumar N, Pandey LM (2018) Removal of methylene blue dye from aqueous solution using immobilized *Agrobacterium fabrum* biomass along with iron oxide nanoparticles as biosorbent. *EnvironSci Pollut Res* 25:21605–21615. <https://doi.org/10.1007/s11356-018-2280-z>

Publisher's Note Springer Nature remains neutral with regard to jurisdictional claims in published maps and institutional affiliations.

Springer Nature or its licensor (e.g. a society or other partner) holds exclusive rights to this article under a publishing agreement with the author(s) or other rightsholder(s); author self-archiving of the accepted manuscript version of this article is solely governed by the terms of such publishing agreement and applicable law.